JOURNAL OF GEOPHYSICAL RESEARCH, VOL. 113, C02S14, doi:10.1029/2007JC004139, 2008

Fast-ice distribution in East Antarctica during 1997 and 1999 determined using RADARSAT data

A. Barry Giles,[1,2] Robert A. Massom,[1,3] and Victoria I. Lytle[4]

Received 1 February 2007; revised 17 May 2007; accepted 2 August 2007; published 12 January 2008.

[1] We present the first detailed maps of fast ice around East Antarctica (75°E–170°E), using an image correlation technique applied to RADARSAT ScanSAR images from November in 1997 and 1999. This method is based upon searching for, and distinguishing, correlated regions of the ice-covered ocean which remain stationary, in contrast to adjacent moving pack ice. Within the overlapping longitudinal range of ~86°E–150.6°E, the total fast-ice area is 141,450 km^2 in 1997 and 152,216 km^2 in 1999. Calibrated radar backscatter data are also used to determine the distribution of two fast-ice classes based on their surface roughness characteristics. These are "smooth" fast ice (−25.4 dB to −13.5 dB) and "rough" fast ice (−13.5 dB to −2.5 dB). The former comprises ~67% of the total area, with rough fast ice making up the remaining ~33%. An estimate is made of fast-ice volume, on the basis of fast-ice type as a proxy measure of ice thickness and area. Results suggest that although fast ice forms 2–16% of the total November sea ice area for this sector of East Antarctica in 1997 and 1999 (average 8.3% across maps), it may comprise 6–57% of the total ice volume (average ~28% across maps). Grounded icebergs play a key role in fast-ice distribution in all regions apart from 150°E–170°E. These are "snapshot" estimates only, and more work is required to determine longer-term spatiotemporal variability.

Citation: Giles, A. B., R. A. Massom, and V. I. Lytle (2008), Fast-ice distribution in East Antarctica during 1997 and 1999 determined using RADARSAT data, *J. Geophys. Res.*, *113*, C02S14, doi:10.1029/2007JC004139.

1. Introduction

[2] Fast ice is an important though poorly quantified and poorly understood component of the Antarctic sea ice cover. In contrast to pack ice, or sea ice that constantly drifts in response to winds, ocean currents and other forces, fast ice is sea ice that remains fixed or "fast" along the coast or close to the coast. It is typically attached to grounded icebergs [*Massom et al.*, 2001a], the shore, an ice wall or an ice front [*World Meteorological Organization*, 1970], and also forms in sheltered coastal embayments, between islands and behind coastal protrusions such as floating glacier tongues. It can also either be annual or perennial, the latter occurring in more sheltered locations. Annual fast-ice breakouts occur during storms [*Heil*, 2006], and/or by the effects of ocean swell penetration [*Crocker and Wadhams*, 1989; *Langhorne et al.*, 2001], the latter typically when the protective surrounding pack ice has dispersed. Although this mainly occurs in spring-summer-autumn [*Ushio*, 2006], intermittent breakouts are not uncommon in certain areas in winter [*Heil*, 2006]. An important overall feature of fast ice is its tendency to recur and persist in given locations.

[3] Earlier work estimated that fast ice accounts for only about 5% (or 0.8×10^6 km^2) of the total Antarctic sea-ice areal extent in November (the typical month of maximum fast-ice extent) [*Fedotov et al.*, 1998]. However, it has a major though poorly understood impact on high-latitude atmosphere-ocean interaction and biological and ecological processes, and forms an important interface between the ice sheet and moving pack-ice zone. Fast and pack ice are often also separated by recurrent flaw leads, which are sites of intense heat exchange and high rates of sea ice formation. Fast ice can also form a boundary for polynya formation [*Massom et al.*, 1998a], again affecting regional rates of sea ice formation and associated water mass modification and formation. Developing an improved understanding of fast-ice distribution and behavior, and its seasonal to interannual variability, is important for a number of reasons. It is sensitive to oceanic and atmospheric forcing, and as such may be a sensitive indicator of climate change and/or variability [*Heil*, 2006; *Murphy et al.*, 1995]. It can grow to a considerable thickness (>5 m), particularly in the case of perennial fast ice, and represents a significant freshwater store to form a major component of the ocean freshwater budget. Moreover, fast ice forms an important habitat for microorganisms [*Arrigo et al.*, 1993; *Garrison*, 1991;

[1] Antarctic Climate and Ecosystems Cooperative Research Centre, c/o University of Tasmania, Hobart, Tasmania, Australia.
[2] Also at Spurion Technology Pty. Ltd., Mt. Rumney, Tasmania, Australia.
[3] Also at Australian Antarctic Division, Kingston, Tasmania, Australia.
[4] Norwegian Polar Institute, Polar Environmental Centre, Tromso, Norway.

0148-0227/08/2007JC004139$09.00

McMinn et al., 2000] and a stable breeding platform for various mammal and bird species for example, Weddell seals (*Leptonychotes weddellii*) and Emperor penguins (*Aptenodytes forsteri*) [*Kooyman and Burns*, 1999; *Kirkwood and Robertson*, 1997]. Finally, it can impede ship access to coastal bases.

[4] While some localized work has been carried out to measure and monitor fast-ice properties and formation/break-up behavior at various locations around Antarctica, for example, at Davis Station [*Heil*, 2006; *Heil et al.*, 1996], in Lützow-Holm Bay [*Enomoto et al.*, 2002; *Ushio*, 2006] and in the South Orkney Islands [*Murphy et al.*, 1995], relatively little is known about its circumpolar extent and large-scale behavior and interannual variability. To date, the most complete map of fast ice around the East Antarctic coast has been that of *Kozlovsky et al.* [1977], described and reproduced in *Fedotov et al.* [1998]. This product, which covered the zone 0°–160°E, was compiled from multiple data sources dating back to the 1970s and earlier. Most of the data used were obtained by visual observation from aircraft flights, resulting in suboptimal spatial and temporal coverage. Satellites provide a much broader pseudo-instantaneous overview to extend these detailed though spatially limited observations. Japanese scientists have extensively used 1-km-resolution National Oceanic and Atmospheric Administration (NOAA) Advanced Very High Resolution Radiometer (AVHRR) data to monitor Antarctic fast-ice distribution in Lützow-Holm Bay (at ~69.2S, 37.5°E and adjacent to Syowa Station) and along the nearby Prince Olav Coast [*Yamanouchi and Seko*, 1992], and to determine factors affecting its break-up behavior [*Ushio*, 2006]. *Enomoto et al.* [2002] used higher-resolution ADEOS Advanced Visible/Near Infrared Radiometer (AVNIR) data to examine breakup and melt, also at Lützow-Holm Bay. Unfortunately, visible to thermal IR sensors, both high resolution such as those onboard SPOT and Landsat satellites and medium resolution, for example, AVHRR and Moderate Resolution Imaging Spectrometer (MODIS), are limited by their inability to penetrate cloud cover and, in the case of visible to near-infrared channels, their reliance on solar illumination [*Lubin and Massom*, 2006]. Although they are unaffected by clouds and darkness, current passive microwave radiometers are generally not suited to fast-ice mapping and monitoring. This is due to their poor resolution, i.e., 6.25–25.0 km for sea-ice concentration products, relative to the seaward extent of fast ice (typically kilometers to tens of kilometers), and pixel contamination with ice sheet signatures in coastal regions.

[5] Spaceborne synthetic aperture radar (SAR) largely overcomes these deficiencies by combining an ability to penetrate polar darkness and cloud cover with a high spatial resolution of tens of meters. While first-generation spaceborne SARs, for example, onboard ERS-1, ERS-2 and JERS-1, were limited in their large-scale mapping/monitoring capability by their narrow-swath coverage of ~100 km width, much-improved coverage came with the launch of ScanSAR technology onboard RADARSAT-1 in 1995 [*Lubin and Massom*, 2006]. This provides good regional-scale coverage over a swath that is up to 500 km wide. Although spaceborne SARs are well-suited to measuring the distribution of fast ice, the latter is often indistinguishable from surrounding pack ice based upon analysis of normalized backscatter values alone in single snapshot images. In this paper, we adapt a feature-tracking method originally developed to measure glacier and ice sheet motion to distinguish stationary fast ice from moving pack ice, in order to map the areal extent of fast ice in East Antarctica sequences of coregistered RADARSAT-1 ScanSAR image pairs. This technique is used to produce detailed "benchmark" maps of fast-ice extent along the coast between 75°E and 170°E for November in 1997 and 1999. We also classify the fast ice on the basis of its surface roughness/backscatter characteristics, to produce estimates of ice volume. Finally, we examine the key characteristics of the fast-ice maps by focusing on certain regions.

2. Data Analysis Methods

[6] In this study, we use ScanSAR Wide images from the C-band (5.3 GHz, wavelength ~5.6 cm, HH polarization) SAR onboard RADARSAT-1, processed by the NASA Alaska Satellite Facility and acquired from NASA's Earth Observing System Data Gateway. The nominal spatial resolution is 50 m. Images are chosen from November 1997 and 1999 for the sector of the Australian Antarctic Territory from 75°E to 170°E, based upon data availability. November is the time of maximum fast-ice extent prior to the austral summer melt/break-up season [*Fedotov et al.*, 1998; *Heil*, 2006].

[7] While interferometric processing of suitable SAR image pairs, i.e., repeat-pass SAR interferometry, shows some promise as a means of detecting and mapping fast ice [*Morris et al.*, 1999], this technique is not exploited here owing to the long temporal baseline (temporal separation between image pairs) and the concomitant lack of suitable coherent image pairs. Rather, fast-ice areal extent is determined by applying a feature-tracking algorithm to coregistered pairs of SAR images, separated in time by 1–20 days (see Tables 1 and 2). Cross-correlation techniques in particular are well suited to such analysis and can be carried out in the spatial domain. Fast Fourier Transform (FFT) techniques in the frequency domain are more efficient, however, when working with larger images. The method used in this study is based upon the public domain IMCORR (IMage CORRelation) software package [*Bindschadler and Scambos*, 1991; *Gray et al.*, 1998]. The technique employed here utilizes previously developed software (A. B. Giles and N. Young, personal communication, 1997) which used the IMCORR engine, embedded in additional controlling code, to map Antarctic glacier velocities. However, for the work presented in this paper, we search for near-zero displacement correlations rather than significant nonzero velocities. Essentially the displacement vectors previously rejected now become the ones of interest assuming that they occur over the ocean; that is, fast ice is reasonably assumed to be motionless.

2.1. Image Preprocessing and Pair Selection

[8] Suitable uncalibrated and nongeocoded RADARSAT-1 ScanSAR images from the East Antarctic coast in 1997 and 1999 were acquired from the NASA Alaska Satellite Facility (ASF). Although the images were mainly from November, a few were used from early December in order to cover the entire coastline of interest. The raw images were binned up by a factor of 4 to give a pixel resolution of

Table 1. RADARSAT Image Pairs Used to Construct the 1997 Map Shown in Figures 4 and 10

Pair Number[a]	Image	Time (UT)	Date	Δ, days
1	R1_10448_651	1535	4 Nov	
	R1_10462_651	1506	5 Nov	0.98
2	R1_10430_711	928	3 Nov	
	R1_10673_711	932	20 Nov	17.00
3	R1_10473_721	941	6 Nov	
	R1_10673_721	933	20 Nov	13.99
4	R1_10606_631	1653	15 Nov	
	R1_10702_716	1015	22 Nov	6.72
5	R1_10435_626	1743	3 Nov	
	R1_10702_726	1016	22 Nov	18.69
6	R1_10421_621	1812	2 Nov	
	R1_10464_621	1824	5 Nov	3.01
7	R1_10607_621	1833	15 Nov	
	R1_10650_621	1845	18 Nov	3.01
8	R1_10436_616	1923	3 Nov	
	R1_10617_731	1132	16 Nov	12.67
9	R1_10622_621	1944	16 Nov	
	R1_10722_621	1940	23 Nov	7.00
10	R1_10408_621	2022	1 Nov	
	R1_10604_621	2013	15 Nov	13.99
11	R1_10408_621	2022	1 Nov	
	R1_10437_621	2104	3 Nov	2.03
12[b]	R1_10437_621	2104	3 Nov	
	...	...	...	...
13	R1_10437_621	2104	2 Nov	
	R1_10723_621	2121	23 Nov	20.01
14	R1_10623_622	2125	16 Nov	
	R1_10723_621	2121	23 Nov	7.00
15	R1_10466_621	2146	5 Nov	
	R1_10666_626	2138	19 Nov	13.99

[a]Image pairs run from Cape Wild (151°E) in the east to the Amery Ice Shelf (75°E) in the west.

[b]A gap of ~130 km is present between 104°E and 107°E. This was filled using a spacer image from 1997.

200 m before the visual selection process commenced. This binning process was carried out to suppress image speckle noise while retaining sufficient resolution for small-scale correlation matches. Where possible, images were chosen with a substantial spatial overlap to facilitate image mosaic construction, and containing prominent coastal features to aid image coregistration. Although an attempt was made to keep the time gaps between images to within 2~7 days, this was often not possible. However, image pairs separated by intervals of several weeks proved usable owing to the persistence and relative stability of the fast-ice cover in November. Details of the 15 image pairs chosen for the 1997 map are given in Table 1. The selection of images for the 1999 map was a completely independent process and images were not always available to cover exactly the same subsections of coastline. Details of the 12 image pairs for the 1999 map are given in Table 2. The regional location of the two maps is shown in Figure 1.

2.2. Image Registration, Correlation, and Masking

[9] For each image pair, the earlier image was defined as the "master" and the second ("slave") image was geometrically warped to match it (using the ENVI (Environment for Visualizing Images) software package). The registration points selected for the warping are on the coastline and the edges of glaciers, since their motion can generally be neglected over periods of a few days. Grounded icebergs were not used for this purpose, given their tendency to rock and/or rotate. Inland registration points cannot be used because of complications associated with linear shifts due to SAR slant-range effects when using points above sea level [*Olmsted*, 1993]. Although relatively few tie-points are available, we are confident about most of the image registrations (based upon close visual inspection).

[10] For the correlation comparison, we define a rectangular and regularly spaced array of points to define the centers of each analysis. This grid of points, taken here to be 8 pixels (i.e., 1600 m) apart, is set up on the master image to cover the entire overlapping region of the two images. For the IMCORR runs, we used a reference tile size of 16 × 16 pixels and a search tile of 64 × 64 pixels. The grid spacing therefore provides a 50% overlap. The IMCORR software searches for a high correlation value of the reference tile on the "master" image within the larger search-tile perimeter on the "slave" image. Since we are searching for zero-velocity features, the IMCORR offset feature was always set to zero to centre the search tile at the expected match location. Although this automatically limits the magnitude of any possible match displacements, this is of no concern for the present application. The correlation analyses can only find matches if both images contain sufficient "structural" detail. For a valid match, the correlation map in IMCORR needs to be clearly single-peaked with a "quality" factor above some limiting value set in the program. The sizes of the reference and search tiles chosen are therefore something of a compromise, dependent on the amount of small-scale detail and "sharpness" present in both images. Suitable values for the tile sizes were chosen after initial experimentation and then retained for the entire mapping process to maintain consistency. Inevitably, some regions of fast ice may appear to contain gaps or holes,

Table 2. RADARSAT Image Pairs Used to Construct the 1999 Map Shown in Figures 5 and 10

Pair Number[a]	Image	Time (UT)	Date	Δ, days
1	R1_21011_622	1759	13 Nov	
	R1_21011_623	1755	26 Nov	13.00
2	R1_21178_729	1037	25 Nov	
	R1_21297_620	1816	3 Dec	8.32
3	R1_20978_728	1045	11 Nov	
	R1_20997_617	1828	12 Nov	1.32
4	R1_21083_616	1853	18 Nov	
	R1_21126_616	1906	21 Nov	3.01
5	R1_21069_621	1923	17 Nov	
	R1_21269_621	1915	1 Dec	13.99
6	R1_21198_616	2000	26 Nov	
	R1_21212_621	1931	27 Nov	0.98
7	R1_21041_618	2022	15 Nov	
	R1_21241_620	3013	29 Nov	14.41
8	R1_21070_620	2104	17 Nov	
	R1_21170_620	2100	24 Nov	7.00
9	R1_21099_616	2145	19 Nov	
	R1_21156_620	2129	23 Nov	3.99
10[b]	R1_10466_621	2146	5 Nov	
	...	...	...	...
11	R1_21128_621	2228	21 Nov	
	R1_21228_619	2223	28 Nov	7.00
12	R1_21128_626	2228	21 Nov	
	R1_21228_626	2224	28 Nov	7.00

[a]Image pairs run from Cape Adare (170°E) in the east to Cape Penck (88°E) in the west.

[b]A gap of ~140 km is present between 87.5°E and 90.75°E. This was filled using a spacer image from 1997.

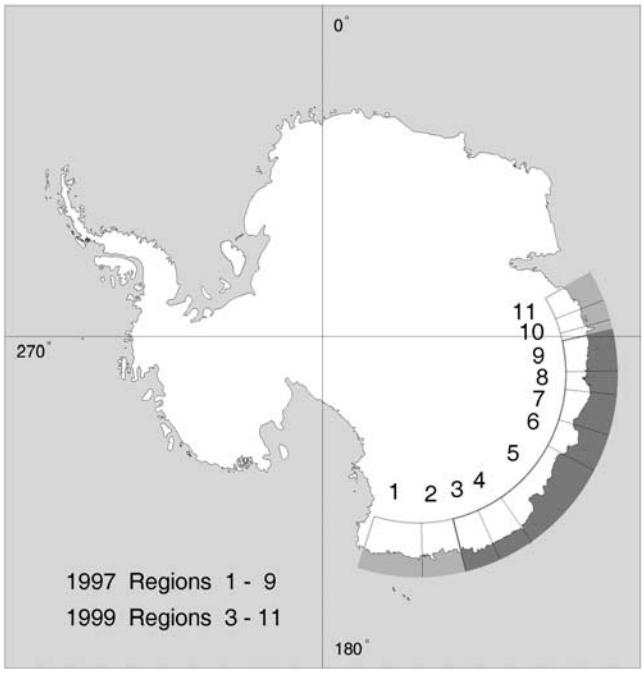

Figure 1. A chart of Antarctica showing the locations of the 1997 and 1999 maps plus the defined regions 1–11 around the East Antarctic coast.

possibly extensive in nature, where correlations are not found but which can be assumed to be fast ice.

[11] The next stage involved constructing a land mask from the master image, in order to filter out all of the land grid points for which valid IMCORR correlations were obtained. A fast-ice mask was then prepared by simultaneously viewing the remaining IMCORR displacement vectors overlaid on the master RADARSAT image. If the displacement vectors are color coded into those below some small limit (i.e., the stationary matches) and those showing larger velocities, then the fast-ice edge can be traced out while visually interpreting the underlying SAR image and making some allowance for gaps in the correlation field. Both black-white fast ice and land masks were also converted to line-edge versions for later use. An example illustrating the processing steps outlined above is presented in Figure 2. This image shows a close-up of the annual fast ice that forms on the Adélie Land coast offshore from the French base Dumont d'Urville. The ice sheet is masked out. The vectors with an absolute magnitude of <1.75 pixels denote the stationary fast ice (low velocity) and are shown as short white vectors (effectively dots). Vectors of >1.75 pixels denote occasional random matches at greater velocity and are shown in black.

2.3. Scatterplot for Registration Check

[12] The output file from an IMCORR run for a pair of images contains a set of pixel displacements between the two images at all of the specified grid points. This file can be displayed as an X-Y displacement scatterplot, as shown in Figure 3, and this was used to classify the vectors in Figure 2 into the two groups. Vectors with absolute magnitudes of <1.75 pixels are shown as black dots, while those with values of >1.75 pixels are grey dots. The tight scatter distribution indicates that: (1) the basic technique works effectively, since many matches are found over the ocean to indicate the presence of extensive fast ice (where expected); and (2) the images were accurately coregistered prior to the correlation analysis. In fact, any slight coregistration error can be removed by recentering the axes to place the peak of the scatterplot at zero. Although the scatter distribution is

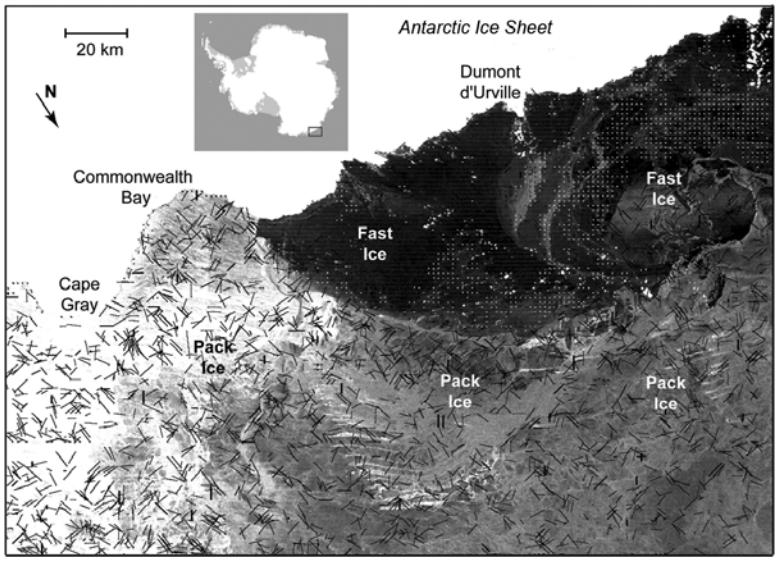

Figure 2. An example of results from the image-correlation technique used to distinguish stationary fast ice from moving pack ice. This example shows the region of annual (first-year) fast ice off the Adélie Land coast at ~138°E–142°E, which forms part of region 4 in Figures 4 and 5. The radar image beneath the correlation motion vectors is R1_10421_621 from 2 November 1997, which was compared with R1_10464_621 from 5 November 1997 (image pair 6 in Table 1). RADARSAT imagery ©Canadian Space Agency/RADARSAT International, 1997.

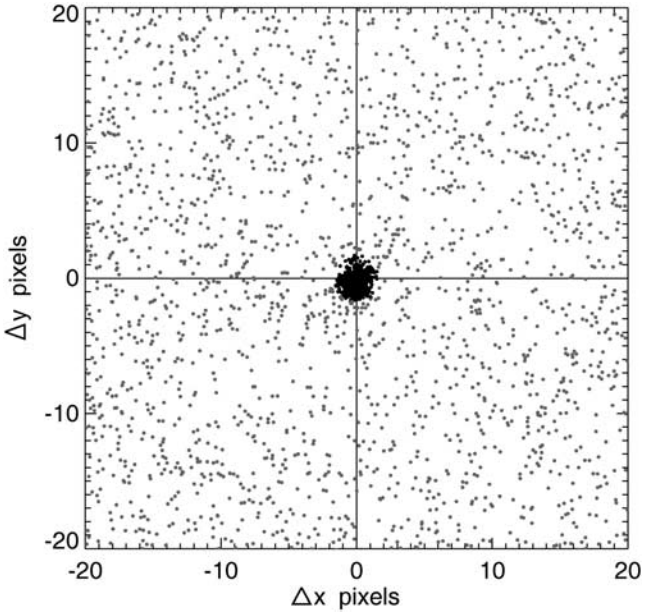

Figure 3. A scatterplot of the image correlation values for the scene in Figure 2. Potential matches over the Antarctic Ice Sheet are eliminated by a land mask. The tight cluster of low displacements (absolute magnitude <1.75 pixels) represents near-stationary features, i.e., fast ice (where 1 pixel = 200 m). There are occasional nonphysical random correlation matches in the moving pack ice (>1.75 pixels).

significantly less symmetrical for some of the image pairs compared to that shown in Figure 3, it is usually well clustered. A few scatterplots show evidence of bimodal clustering. Inspection of the associated SAR images and displacement vectors shows that this results from intermittent slippage of slabs of fast ice farthest offshore between the dates of the two images.

[13] The "background" of grey dots in Figure 3 does not reflect "real" pack ice motions. Random matches are occasionally obtained from the correlation analysis, with their number depending on the amount of structure in the images, their sharpness and signal-to-noise ratio, and the threshold setting used by IMCORR to define an acceptable tile match. In Figure 3, there are 1866 vectors within the tight cluster, with a background rate of only 15 implied from the density of grey dots, i.e., a large spike on a low and fairly flat background.

[14] Many of the smaller icebergs present within or close to the coastal fast-ice zone are also stationary over intervals of a few days and beyond, and any tiles encompassing them, or a part of them, will also give correlation matches. Therefore some areas containing iceberg fields can contribute many matches to the cluster, leading to a slight overestimate for fast-ice area. The issue of small icebergs encouraging the formation and trapping of fast ice or, alternatively, fast ice trapping small icebergs, is discussed in section 3.

2.4. Geometric Representation of Mosaiced Image Pairs

[15] Once processed, the image pairs were combined to form the two mosaic maps, i.e., for 1997 and 1999. This step encountered the problem of representing an extended series of images, which follow a curved track, on the surface of a sphere. Since the East Antarctic coastline is an approximately circular sector, albeit not centered on the South Pole itself, we experimented using a mapping system based on approximating the mean coastline to a series of simple line segments which were subsequently straightened out. The main problem in representing the map in this way is that the sense of curvature of the coastline at the line segment joins leads to stretching or compression away from the coast. This effect becomes more pronounced with distance offshore along the joint line. For this reason, the joins were placed between regions having any extensive offshore fast ice. The resulting regions (1–11 in Figure 1), are almost identical for the two maps and are unrelated to the image pair numbering sequences given in Tables 1 and 2.

[16] The next step involved calibration of the initial RADARSAT images, using the standard ASF SAR calibration software [*Martyn et al.*, 1999]. These images were then transformed to exactly match their uncalibrated versions, and the complete set was built into mosaics that were spatially equivalent to the uncalibrated maps. The composite calibrated RADARSAT maps of fast-ice distribution for November 1997 and 1999 are shown in Figures 4a and 5a, respectively. These "snapshot" maps cover the East Antarctic coast from 87.5°E–170.3°E for 1997 and 75.15°E–150.61°E for 1999.

[17] Information on ocean bathymetry was derived from *Porter-Smith* [2003] and the NOAA National Geophysical Data Center Terrainbase Land and Sea Elevation data set (5 × 5 minute resolution), obtained from http://www.marine.csiro.au/~mansbrid/dods/climatology.html. The 250-m contour was chosen as this approximates the maximum depth at which East Antarctic icebergs typically ground [*Massom*, 2003]. The fine-resolution coastline was extracted from the Data Centre archive of the Australian Government Antarctic Division (AGAD), carefully defined in order to avoid the inclusion of sea ice. Another task was to identify the exact positions of the ends of the string of line segments used to construct the 1997 and 1999 maps. These locations were identified on the AGAD coastline data set and a geometrical construction method was used to determine the perpendicular distance to the adjacent section of the bathymetry contour while traversing each line segment. These strings of "offshore" distances (in effect distances from the line segment) were then used to define the position of the bathymetry contour on the new 1997 and 1999 map projections.

3. Results

3.1. Fast-Ice Areal Extent

[18] The derived maps of fast-ice extent for both 1997 and 1999 are shown in Figures 4b and 5b, respectively. In November 1997, the total fast-ice area of 162,788 km^2 for the entire sector 87.5°E–170.3°E equates to an average equivalent offshore distance of 43 km along the entire mapped coastline. In fact, the actual offshore distance ranges from a few kilometers to ~150 km, for example, at ~100°E and 129°E. In 1999, the "snapshot" covers the coastal sector 75.15°E–150.61°E, and the total fast-ice area is 168,068 km^2. This equates to an average equivalent offshore distance of 48 km along the entire mapped coast-

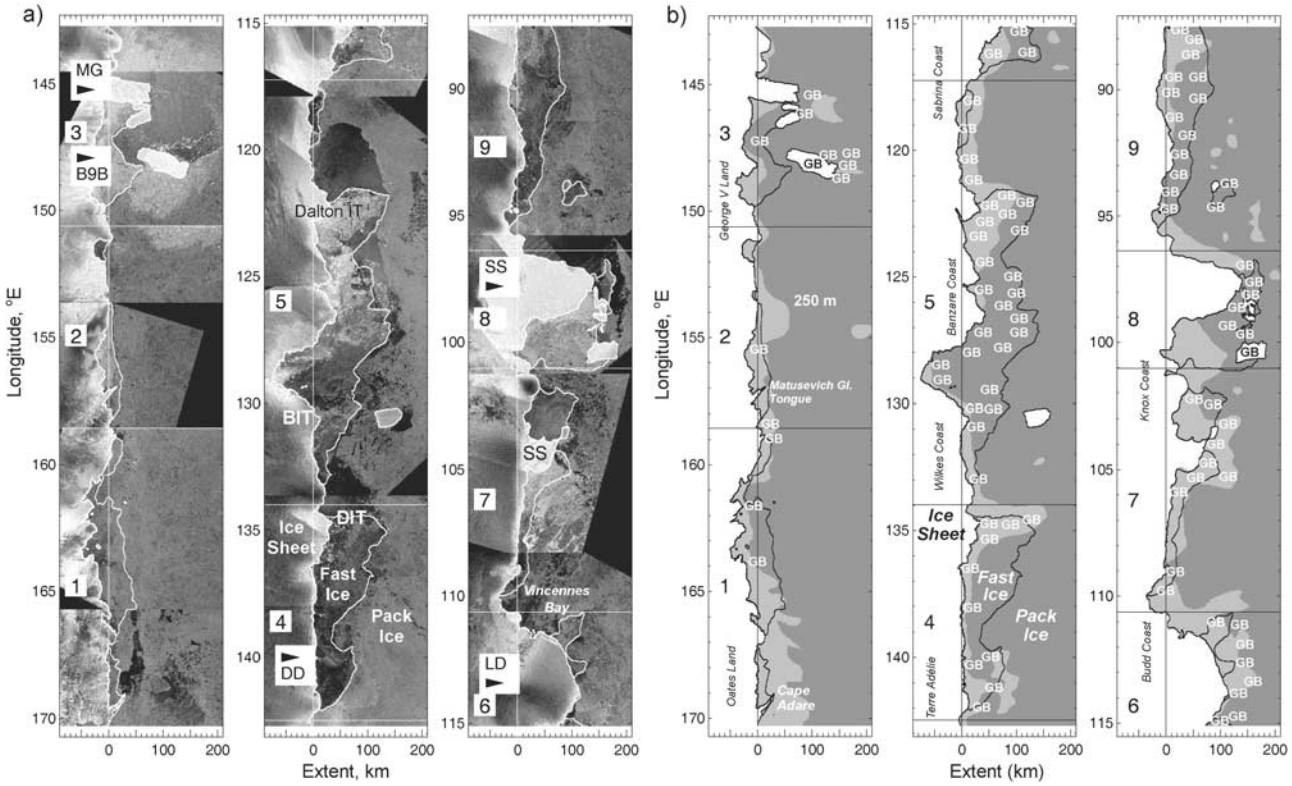

Figure 4. (a) Mosaic of RADARSAT ScanSAR images from November 1997 around the East Antarctic coastline from 87.5°E to 170.3°E. This is overlain with lines defining the coastline mask and the extent of the fast ice as determined by the image correlation method. A number of well-known features are provided for visual reference, i.e., iceberg B-9B (B9B), Mertz Glacier tongue (MG), Dumont d'Urville (DD), Law Dome (LD), Shackleton Ice Shelf (SS), and Dibble Iceberg Tongue (DIT). Regions 1∼9, denoted by the white line longitude dividers, are discussed in the text. Details of the ScanSAR image pairs used are given in Table 1. (b) Map of derived fast-ice distribution for November 1997. Ocean depths of ≤250 m are shown in light grey. The locations of approximate assemblages of grounded icebergs are marked GB. RADARSAT imagery ©Canadian Space Agency/RADARSAT International, 1997.

line. Once again, the actual distance ranges from a few kilometers to ∼150 km (in this case at ∼84°E, 100°E, 129°E and 149°E).

[19] A comparison is made between fast ice and pack ice extent. Sea ice extent data were obtained from monthly mean ice concentrations derived from application of the NASA Bootstrap algorithm [*Comiso*, 1995] to SSM/I brightness temperature data, where the ice edge is taken to be the 15% concentration isoline. In Table 3, we show the November mean sea ice area within each region (1–11) extracted from the SSM/I images and the relative proportions of fast ice. The ratios of the fast-ice area (Table 4) to the sea ice areas in Table 3 are plotted in Figure 6. These range from ∼2% to 16%, with averages of 8.3% and 8.4% for 1997 and 1999 respectively. For the 7 overlapping regions (2–9) where a comparison between 1997 and 1999 can be made, we see in Table 3 that regions 3, 4 and 8 differ substantially. Differences in the fast ice to sea ice ratio may occur owing to changes in the fast-ice area, the sea ice area or from both. Comparison of Tables 3 and 4 shows that the ratio change in region 3 (George V Land) is primarily due to an approximate doubling of fast-ice area from 1997 to 1999. Conversely, for region 4 (Terre Adélie), there is an approximate halving of the fast-ice area in 1999 compared to 1999. The smaller, but still significant, change in the ratio for region 8 (Shackleton Ice Shelf) is due to both an increasing area of sea ice and a decreasing area of fast ice from 1997 to 1999. The smaller changes in Table 3 (of <5 sigma) are probably not significant owing to the various approximations and systematic effects inherent in deriving the sea ice area, the fast-ice area and the relative overlap due to mapping issues related to the SSM/I pixel scale and quantization. Once again, it must be stressed that these are "snapshot" estimates only.

[20] In total, fast ice in the two overlapping coastal sectors studied (i.e., 3–9) accounts for ∼9.9% and 9.5% of the total sea ice areal extent as an average across the region ∼85°E–151°E in 1997 and 1999, respectively. This compares with 5% for total Antarctic sea ice estimated by *Fedotov et al.* [1998].

[21] Information on ocean bathymetry is included in Figures 4b and 5b to highlight the strong relationship between fast-ice distribution and ocean depth. The approximate locations of assemblages of grounded icebergs, derived from detailed inspection of the ScanSAR composite mosaics and motion information from the image time series, are marked GB in Figures 4b and 5b. Comparison with the patterns of fast-ice distribution reveals the key role of

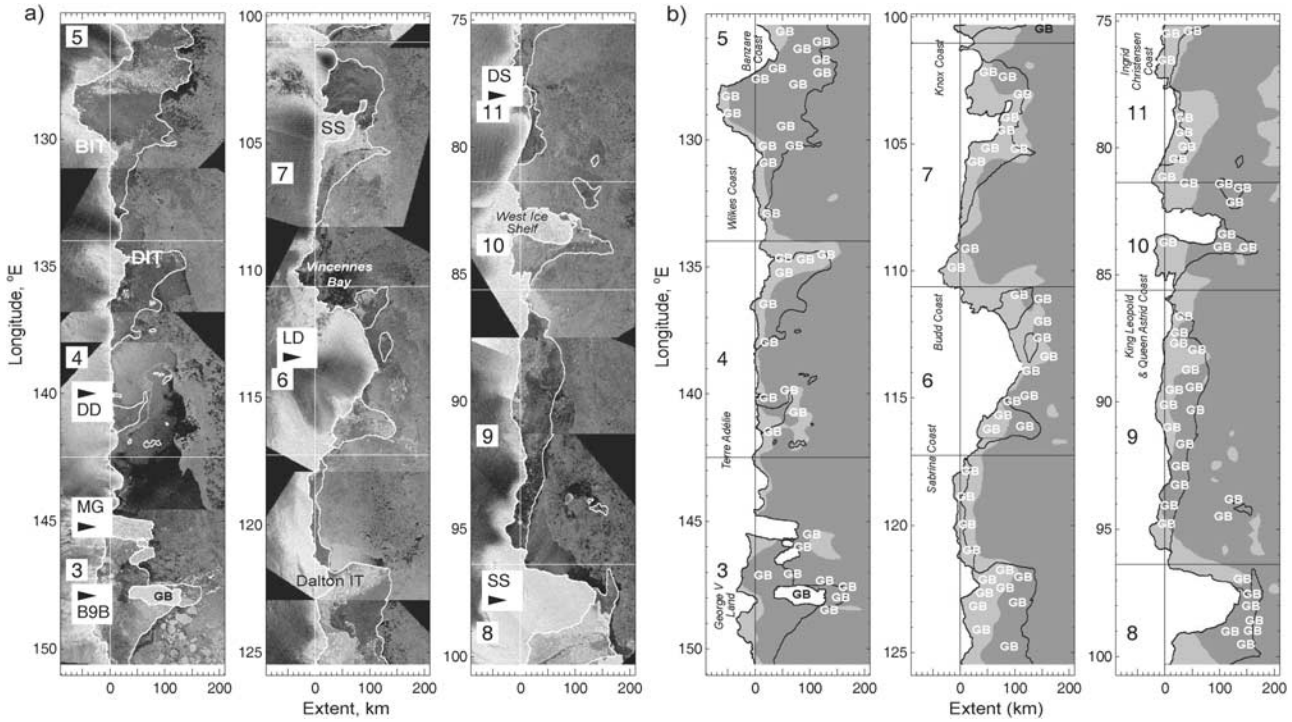

Figure 5. (a) Mosaic of RADARSAT ScanSAR images from November 1999 around the East Antarctic coastline from 75.2°E to 150.6°E. This is overlain with lines defining the coastline mask and the extent of the fast ice as determined by the image correlation method. A number of well-known features are provided for visual reference, i.e., iceberg B-9B (B9B), Mertz Glacier tongue (MG), Dumont d'Urville (DD), Law Dome (LD), Shackleton Ice Shelf (SS), and Dibble Iceberg Tongue (DIT). Regions 1–9, denoted by the white line longitude dividers, are discussed in the text. Details of the ScanSAR image pairs used are given in Table 2. (b) Map of derived fast-ice distribution for November 1997. Ocean depths of ≤250 m are shown in light grey. The locations of approximate assemblages of grounded icebergs are marked GB. RADARSAT imagery ©Canadian Space Agency/RADARSAT International, 1997.

grounded icebergs as "anchor points" for fast-ice formation, particularly along coastal sectors with few coastal promontories or sheltered embayments [*Massom et al.*, 2001a]. Figure 7 [after *Massom*, 2003] focuses on the George V Land coast sector of region 3 to illustrate the importance of small, in addition to large, grounded icebergs. A prominent feature of the region to the east of the floating Mertz Glacier Tongue is iceberg B-9B. This vast iceberg, which calved from the Ross Ice Shelf in October 1987, grounded in approximately its current position in June 1992 [*Keys*, 1994]. It effectively combines with accumulations of small icebergs grounded on Ninnis Bank and marked SGB1 in Figure 7 to form a meridional barrier that extends >250 km from the coast; that is, it extends right across the Antarctic Coastal Current to intercept westward drifting pack ice. This leads to the dynamic accumulation of fast ice on the eastern (upstream) side of the barrier. This flank is separated from the drifting pack by an extraordinary recur-

Table 3. Sea Ice Area, Fast-to-Sea Ice Ratios, Changes and Fast-Ice Percentage Volumes for Both Maps

	Sea Ice,[a] km^2		Fast Ice/Sea Ice,[b] %		σ Fast Ice Volume, %		
Region	1997	1999	1997	1999	1997–1999	1997	1999
1	475,750	456,548	3.38 ± 0.03	...	...	10.6	...
2	261,489	222,956	2.01 ± 0.03	...	...	9.7	...
3	165,680	155,996	5.82 ± 0.07	11.96 ± 0.12	44.3	31.1	39.5
4	155,146	160,385	15.92 ± 0.14	8.64 ± 0.09	42.7	34.4	22.2
5	306,580	351,704	15.55 ± 0.10	16.20 ± 0.10	4.8	45.1	45.7
6	162,063	173,337	5.43 ± 0.07	5.45 ± 0.07	0.2	19.8	22.1
7	264,084	313,588	5.08 ± 0.05	5.42 ± 0.05	4.6	18.0	19.2
8	104,199	117,119	14.78 ± 0.16	11.65 ± 0.13	14.7	52.2	46.3
9	317,477	315,809	6.88 ± 0.06	7.16 ± 0.06	3.3	19.4	20.1
10	167,888	128,635	...	7.10 ± 0.09	...	...	27.8
11	331,816	313,731	...	2.14 ± 0.03	...	...	6.3

[a]Average area during November each year.
[b]Area of "smooth" plus "rough" fast ice.

Table 4. Fast-Ice Area by Region and Type for Both 1997 and 1999[a]

		Smooth, km^2		Rough, km^2		Total, km^2	
Region	Longitude, °E	1997	1999	1997	1999	1997	1999
1	170.30-158.56	13,615	...	2456	...	16,071	...
2	158.56-150.41	2562	...	2705	...	5267	...
3	150.61-142.48	749	10,582	8886	8080	9635	18,662
4	142.48-133.98	23,953	12,763	746	1099	24,699	13,862
5	133.98-117.24	30,272	37,585	17,388	19,405	47,660	56,990
6	117.24-110.63	5908	5170	2899	4283	8807	9453
7	110.63-101.03	9523	11,830	3893	5169	13,416	16,999
8	101.03-96.38	4254	3081	11,148	10,565	15,402	13,646
9a	96.38-87.50	19,102	...	2729	...	21,831	...
9	96.38-85.61	...	19,703	...	2901	...	22,604
10	85.61-81.36	...	4798	...	4340	...	9138
11	81.36-75.15	...	6086	...	628	...	6714

[a]See Figure 10. Region 9a is part of full region 9.

rent shear zone that typically extends to Cape Freshfield to the SE, i.e., a distance of ~150–200 km to the SE. The resultant "wedge" of fast ice and icebergs combined then acts as a protective barrier to create relatively quiescent conditions to the W/SW. Together with the presence of series of grounded icebergs, this promotes additional fast-ice growth, in this case largely by thermodynamic processes. These are joined by icebergs locally calved by glaciers along the coast between the Ninnis and Mertz Glaciers. Under current conditions, icebergs created by a calving of the Ninnis Glacier tongue in 2000 reside in the approximate location marked GB to form significant fast-ice anchor points. Icebergs C-8 and C-9 adjacent to the terminus of the Mertz Glacier are from a previous calving of the Ninnis Glacier, in 1980–1982 [*Frezzotti et al.*, 1998]. These have since dislodged to drift westward. Work by *Frezzotti et al.* [1998] and *Massom* [2003] suggests that the large icebergs produced by the Ninnis Glacier reside in the region for 10–20 years to impact fast-ice distribution. In addition, the assemblages of small grounded bergs marked SGB1 and SGB2 in Figure 7 are conjoined by fast ice throughout the winter months, to extend its meridional coverage to ~67°S.

[22] The central role of small grounded icebergs in fast-ice growth and recurrence is underlined by the fact that the "wedge" was virtually identical in 1963 to the present day, in spite of the fact that B-9B did not drift into the region for another 30 years [*Massom et al.*, 2001a]. This indicates that the myriads of small grounded rather than vast tabular bergs are the key building blocks of fast-ice distribution, each constituting an "anchor point" for growth. Fast ice also has the effect of trapping nongrounded icebergs [*Massom*, 2003].

[23] The relatively narrow band of fast ice along the coast from ~150°E to 170°E to some extent reflects the relative lack of grounded iceberg assemblages in sectors 1 and 2 in 1997 (Figure 4). Grounded icebergs that are there do play a significant role as anchor points, as do coastal promontories and protrusions. An important example of the latter is the Matusevich Glacier Tongue at ~157.45°E, 69.34°S, a feature that extended seaward by ~30 km in 1997. Similarly, Cape Adare forms the eastern boundary of fast ice along the Oates Land Coast at ~170°E. Well-developed recurrent flaw leads commonly occur along the northern boundary of the fast ice in these sectors.

3.2. Identification of Fast-Ice Types

[24] A second aspect of the study was to classify fast-ice types on the basis of their calibrated radar backscatter characteristics. An example of a subregion from a calibrated image is shown in Figure 8a. This section of coastline is near Cape Elliott and Bowman Island at a longitude of ~101°E–107°E. The 0- to 255-byte values in the image now scale directly to the SAR backscatter power values, where 0 is −25.5 dB and 255 is 0 dB. A histogram of the intensity values within the two fast-ice regions identified in Figure 8a is shown in Figure 9. This clearly indicates a

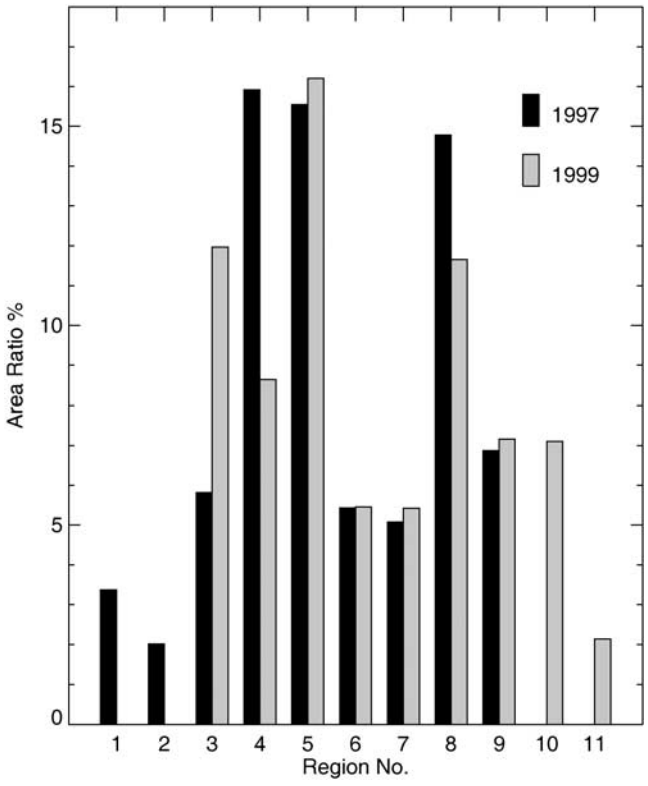

Figure 6. Percentage of the total sea ice area represented by the sum of the smooth and rough fast ice in the 1997 and 1999 maps. The overall sea ice area is derived from DMSP SSM/I ice concentration data. The fast-ice data are extracted from Table 4.

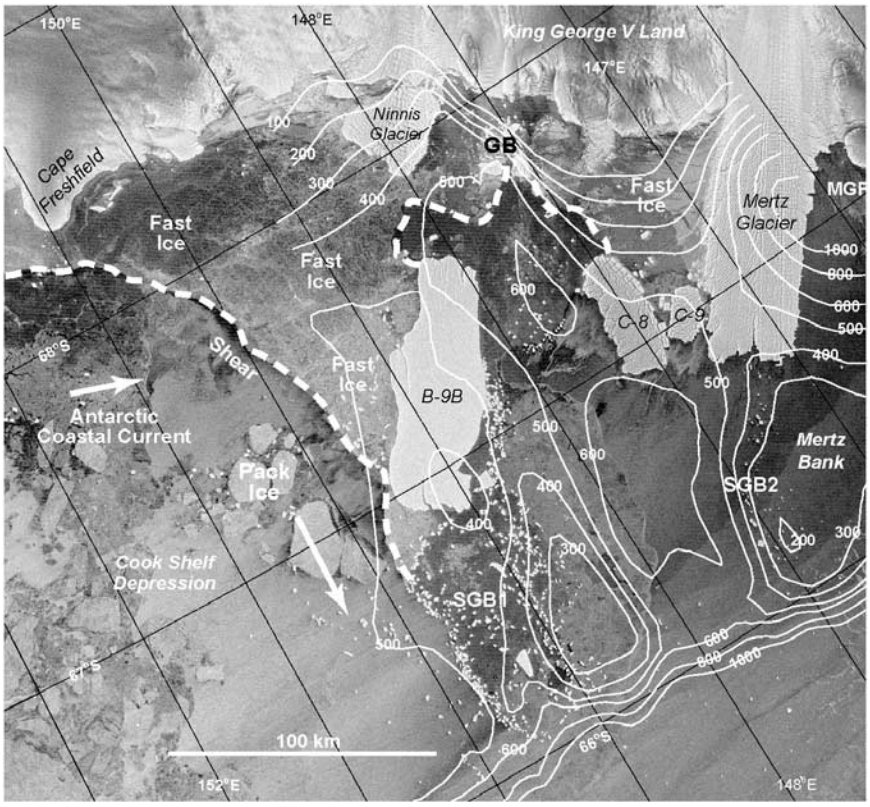

Figure 7. A RADARSAT ScanSAR image from 20 November 1999 of the King George V Land coast region showing the distribution of fast ice and icebergs, with ocean bathymetry contours superimposed. The white dashed line denotes the approximate boundary of fast-ice extent. MGP is Mertz Glacier Polynya, GB grounded icebergs, and SGB (1 and 2) small grounded icebergs. NB Bathymetric contours are not shown to the left of the image (east) owing to the unreliability of ocean depth data in this region. RADARSAT imagery ©Canadian Space Agency/RADARSAT International, 1999.

bimodal distribution, confirming visual analysis of the image that two distinct fast-ice types are present. Thresholding of the image results in a map of the two ice classes, as shown in Figure 8b. One class, depicted in black, relates to relatively smooth ice (backscatter range −25.4 to −13.5 dB), while the other class (depicted in grey) denote areas of rougher ice (backscatter range −13.5 to −2.5 dB). Any apparent half-tone shades are an artifact of the spatial distribution of the two basic classes. A mean threshold value was selected by analysis of equivalent intensity histograms for all of the image pairs used. This is marked as a vertical line on Figure 9. Complete mosaic maps of the distribution of ''rough'' and ''smooth'' fast-ice types derived in this manner are presented in Figure 10a (1997) and 10b (1999).

[25] The ''smooth'' category represents mainly first-year (FY) fast ice with a low backscatter and few textural features in the calibrated C-band SAR imagery. Low backscatter results from specular reflection due to the relative lack of surface-roughness facets. The ''rough'' category, on the other hand, is dominated by diffuse reflection from a rough surface combined with strong volume inhomogeneities within the snow and ice substrate. This results in a significantly brighter radar return. In this case, the ''rough'' fast-ice class comprises two subclasses, namely (1) highly deformed FY ice and (2) thick multiyear (MY) ice with a thick snow cover. This classification is based upon comparison of limited in situ observations during recent research cruises to the region [*Massom et al.*, 2001a] with contemporary calibrated ScanSAR data. As such, an assumption is made about the wider-scale representativeness of the backscatter-ice type relationship. In fact, comparison of Figures 10a and 10b reveals consistency in the distribution of both ice types from year to year, with the exception of region 3 (the area around the Mertz Glacier).

[26] Such a classification would break down during periods of snow cover melt, when the backscatter contrast between ice types is reduced. Periodic melt periods can occur in the region even in winter [*Massom et al.*, 1998b]. This may account for the apparent disappearance of MY fast ice in imagery to the immediate east of the Mertz Glacier (at ~146°E) in 1999 (Figure 10b). On the other hand, multiple seasonal thaw-refreeze cycles and extended temperature-gradient metamorphism experienced by MY fast ice generally result in a snow cover that is granular and contains icy layers [*Massom et al.*, 2001b]. This in turn likely makes a major contribution to the strong backscatter under freezing conditions, as observed in the Mertz Glacier region of region 3 in 1997 (Figure 10a).

[27] Of the two subcategories of ''rough'' fast ice, highly deformed FY ice typically forms by the interception by

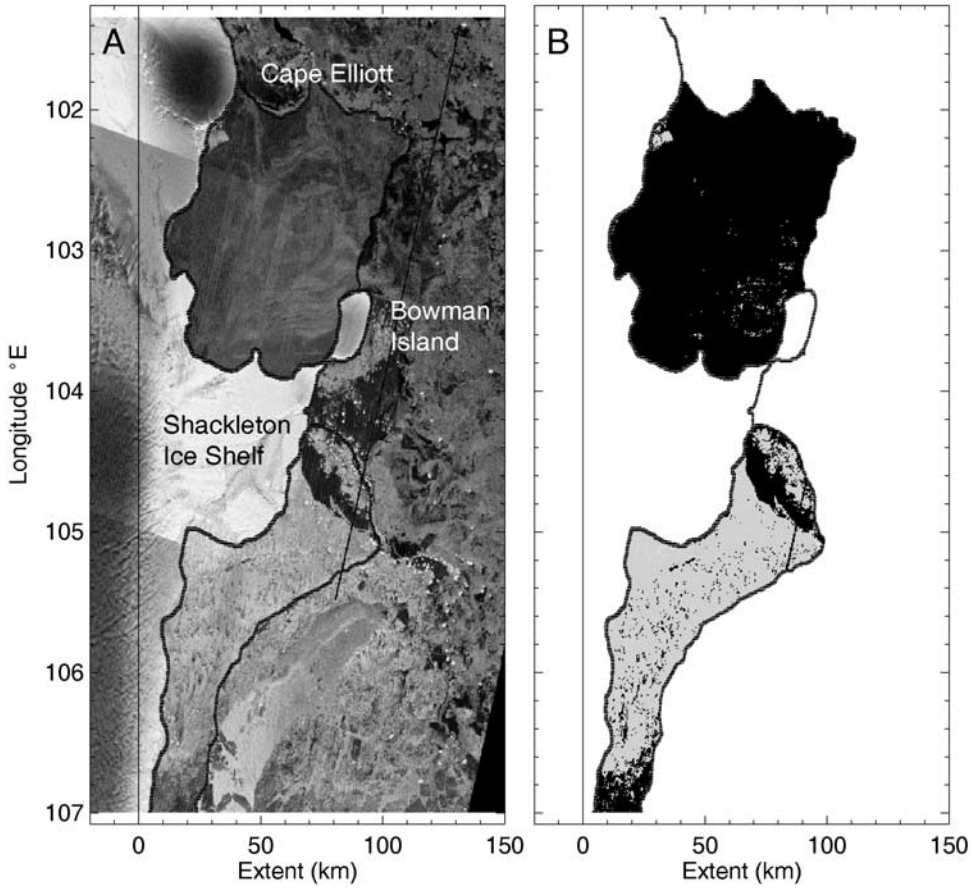

Figure 8. (a) A calibrated RADARSAT ScanSAR image acquired on 3 November 1997 showing a small section of coastline from ~101°E–107°E. This is part of image pair 13 in Table 1, and part of region 7 in Figures 4 and 5. (b) Derived fast-ice regions divided into the two backscatter ranges. The black areas correspond to "smooth" fast ice with backscatter values in the range −25.4 dB to −13.5 dB. The grey areas correspond to "rough" fast ice with higher backscatter in the range −13.5 dB to −2.5 dB. RADARSAT imagery ©Canadian Space Agency/RADARSAT International, 1997.

coastal promontories and grounded icebergs of pack ice drifting westward within the East Wind Drift and, in certain locations, driven by katabatic winds [*Massom et al.*, 2001a]. An example is the region to the immediate east of grounded iceberg B-9B described earlier (see Figures 7, 10a and 10b,). Pack ice that is not deflected to the NW piles up against the eastern flank of this barrier. The resultant "wedge" of highly deformed fast ice comprises one of the major regions of perennial ice in East Antarctica.

[28] Regions of MY fast ice occur in more sheltered embayments, for example, in the SE lee of the Mertz Glacier tongue at ~146°E–150°E, where further protection is afforded by grounded iceberg B-9B and the recently calved Ninnis Glacier icebergs to the N/NE [*Massom*, 2003]. The fast ice in the region 145°E–147°E is at least 9 years old, based on comparison of current with earlier RADARSAT data. In other regions, "smooth" fast ice forms to the western (lee) side of promontories, i.e., in more sheltered locations. An example, of the effect of the Shackleton Ice Shelf (~104°E–105°E) on the formation of "smooth" fast ice to the west and "rough" fast ice to the east, is shown in Figure 8.

3.3. Variability in Fast-Ice Areal Extent and Type Distribution

[29] In this section, we examine spatiotemporal variations in total fast-ice area and the relative proportions of "rough" and "smooth" ice types present for the Novembers of 1997 and 1999. Areas of fast ice (both total and per fast-ice type) are given for the complete image mosaics in Table 5 and for the regional sectors in 1997 (regions 1–9) and 1999 (regions 3–11) in Table 4.

[30] Where spatial overlap occurs between 1997 and 1999, i.e., sectors 3–9, the respective total fast-ice areas are 141450 km^2 and 152216 km^2. This equates to an increase of ~8% in 1999 relative to 1997. Fast-ice area on a type and sector-by-sector basis is compared schematically for 1997 and 1999 in Figure 11, with details given in Table 4. Considerable spatiotemporal variability is noted in total fast-ice extent. While some regions, i.e., 3 and 5–7, exhibit an increase (ranging from 7% for region 6 to 94% for region 3), others show a decrease in 1999 compared to 1997. These are regions 4 (−44%) and 8 (−13%). It is difficult to draw any concrete conclusions from this result, however, given that the data represent "snapshots" in time

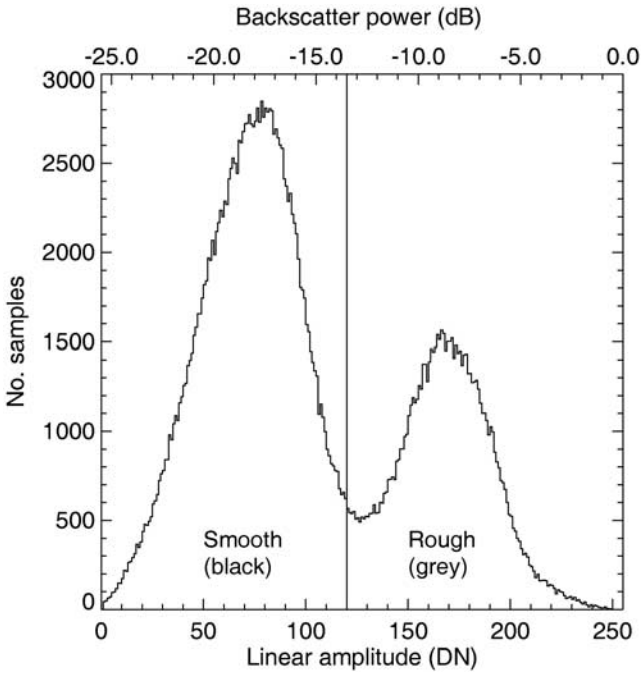

Figure 9. Backscatter intensity histogram for all of the fast ice identified in Figure 8. There is a clear bimodal distribution between the smoother (black) and rougher (grey) fast-ice clusters. The calibrated backscatter (dB) threshold level used for Figure 8, and in the complete maps in Figure 10, is indicated by the vertical line.

only and that changes can occur in response to synoptic-scale atmospheric forcing. However, it does illustrate that considerable interannual variability can occur.

[31] Spatiotemporal variability is also noted in the extent of the two major ice types (see Figure 11), with results summarized in Table 4. For comparison, *Kozlovsky et al.* [1977] estimated that the total area of MY fast ice never exceeds 18000 km^2, in this case over a wider longitudinal sector, i.e., 0°–165°E. This is a significantly lower figure than the sum of those given in Table 4.

[32] It is apparent from Figure 11 that the changes in fast-ice areal extents between 1997 and 1999 are largely due to changes in the area of "smooth"-type ice present. The extent of "rough" ice remains largely consistent between the years. Moreover, the relative proportions of the two ice types remain remarkably stable, i.e., 67.5% versus 66.4% for "smooth" ice and 32.5% versus 33.6% for "rough" ice in 1997 and 1999, respectively. This suggests that "losses" in one region tend to be compensated for by "gains" in other regions. Comparison of the maps from 1997 and 1999 with that from *Kozlovsky et al.* [1977], which is reproduced as *Fedotov et al.*'s [1998] Figure 1, also shows that a close correspondence exists between regions of high SAR backscatter observed in this study and areas of MY fast ice identified in the earlier visual airborne observations. An example is the lens of ice centered on ~105°E (to the east of the Shackleton Ice Shelf, in region 7 in Figure 10). These factors lend further confidence to the classification procedure, although further in situ measurements are required for validation.

[33] The relatively small proportion of MY fast ice in region 4 reflects the lack of coastal promontories in the region. The fast ice in this region is indeed predominantly annual. It forms between series of small and locally produced grounded icebergs that extend ~100 km offshore, including the Dibble Iceberg Tongue at ~135°E. The annual break-up/melt back of fast ice in region 4 occurs with the seasonal removal of the protective pack-ice cover [*Massom et al.*, 2001a]. Major iceberg tongues occur elsewhere at ~122°E (Dalton) and ~131°E (Blodgett), and all are associated with heavy, extensive and in certain cases persistent fast ice.

[34] Variability in fast-ice extent on shorter, for example, synoptic, timescales is an important factor that remains unresolved by the current study, and one that has a subtle though profound impact downstream in the complex Antarctic coastal system. Other work, for example, by *Massom et al.* [2003], has shown for example, that intermittent breakouts (and subsequent reformations) of the eastern flank of the fast-ice "wedge" in region 3 (Figure 7) occur throughout the year and are related to wind direction, with a peak during periods of southwesterly winds and the summer months when the area is unprotected by pack ice. These break-out events create a tongue of MY floes (>5 m thick, determined from in situ observations) that combines with pack ice (steered to the NW by the "wedge"; see the white arrow in Figure 7) and remain compact as these drift westward with the trend of the shelf break to the north of the Mertz Glacier Polynya ~200 km to the SW [*Massom et al.*, 2001a]. This tongue can physically restrict the width of the outlet zone available for the advection of ice created in the polynya out of the immediate region, leading to a "clogging up" of the system and periodic reductions in the polynya size. Given that this important polynya is a major source region of Antarctic Bottom Water formation [*Rintoul*, 1998], the distribution and breakout behavior of fast ice 100s of kilometers "upstream" has implications for global ocean thermohaline circulation and climate. Such is the subtlety and complexity of interactions and processes in the Antarctic coastal zone, where ice sheet and sea ice are intimately linked. Grounded iceberg assemblage SGB2 has a further effect when seasonally conjoined by fast ice by effectively doubling the size of the polynya in the N-S direction, i.e., from ~100 km to ~200 km [*Massom et al.*, 2001a].

[35] Because of the persistence of high winds and associated upper ocean turbulence [*Roberts et al.*, 2001], the immediate vicinity of the Mertz Glacier Polynya itself is largely devoid of fast ice. However, sea ice formed in the polynya is swept westward by katabatic and synoptic winds to make a major contribution to the buildup of the eastern flank of annual fast ice off the Adélie Land coast at ~135°E–142°E (region 4 in Figures 4 and 5; see Figure 2). This again largely occurs by dynamic interception of the pack ice by lines of icebergs grounded on banks to the NE of Dumont d'Urville. The resultant eastward propagation of the eastern fast-ice flank in turn decreases the size of the coastal component of the polynya [*Massom et al.*, 2001a]. Elsewhere, polynya formation occurs in the lee of combined fast-ice-grounded iceberg barriers. Notable examples are the Cape Darnley Polynya at ~69.1°E (67.6°S) and the large recurrent polynya to the west of the Dibble Iceberg Tongue

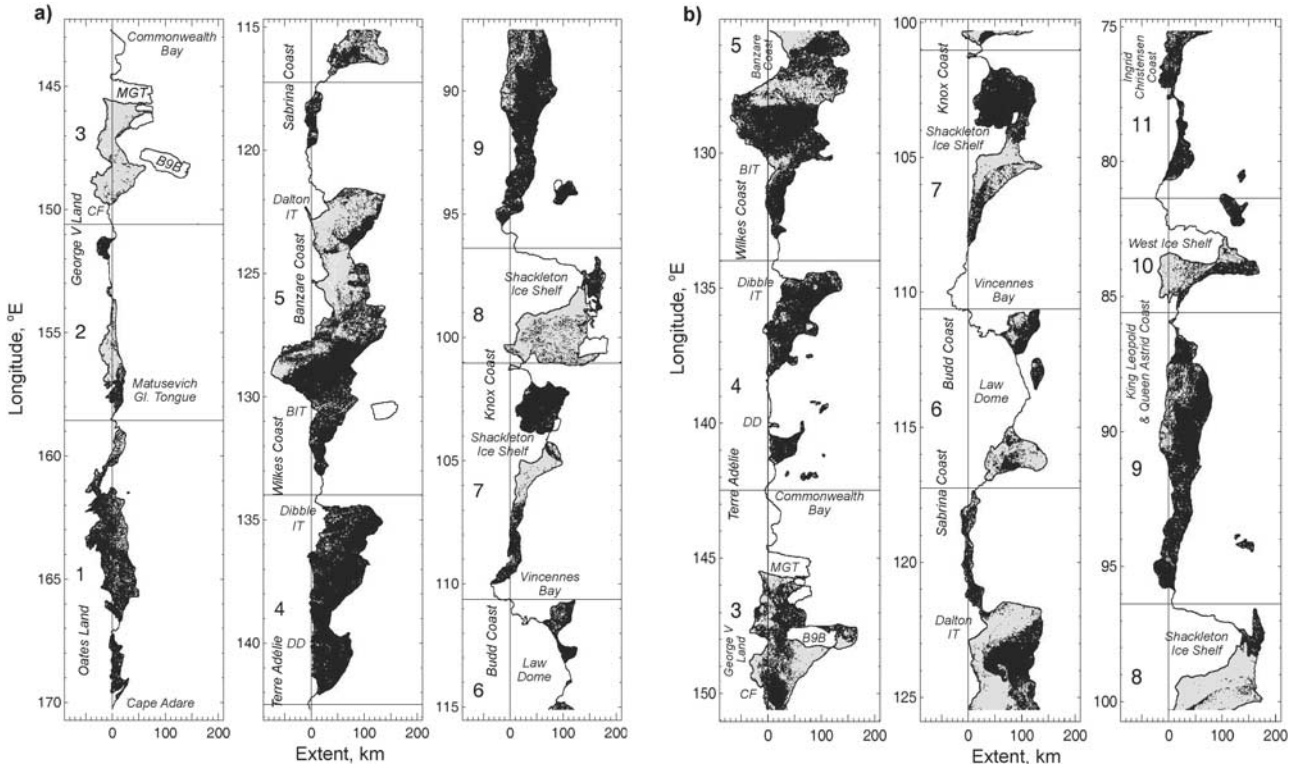

Figure 10. Maps of fast-ice type for (a) November 1997 and (b) November 1999, based on thresholding the calibrated radar backscatter signal. This figure is a companion to Figures 4 and 5, covering exactly the same sections of coastline. Black areas correspond to fast ice with lower backscatter in the range of −25.4 dB to −13.5 dB. Grey areas correspond to rougher/thicker fast ice with higher backscatter in the range of −13.5 dB to −2.5 dB. The longitudinal scale is slightly different for Figures 10a and 10b.

at ∼134.2°E (66.9°S) [*Massom et al.*, 1998a]. By being associated with the formation of certain important polynyas, East Antarctic fast ice plays an important indirect role in determining enhanced regional sea-ice production rates, water mass modification and Antarctic Bottom Water formation [*Bindoff et al.*, 2000], rates of primary production [*Arrigo and van Dijken*, 2003] and the ecology and survival of apex predators [*Massom et al.*, 1998a].

3.4. Estimate of Fast-Ice Volume

[36] In this section, we combine the information on fast-ice areal extent and type presented above with in situ observations of fast ice and sea ice thickness to derive estimates of fast-ice volume. This is based on the assumption that fast-ice type is a proxy broad-scale measure of ice thickness, with thicknesses of 1.7 m and 5.0 m being assigned to "smooth" and "rough" fast ice, respectively. The former derives from the mean annual maximum fast-ice thickness at Davis Station for the years 1979–2003 [*Heil*, 2006], falling as it does in the zone of "smooth" ice in Figure 10. The 5-m thickness is a midrange estimate based on observations during Australian cruises to the Mertz Glacier region in 1998 and 1999 of multiyear fast ice that had broken out from the area to the east of the glacier [*Massom et al.*, 2001a]. The thickness information is then combined with the satellite-derived estimates of overall sea ice extent (see Table 3 and Figure 6) to derive estimates of the relative proportion of sea ice volume contained in fast ice for both 1997 and 1999. Given the uncertainties in representative ice thickness and its variability as a function of ice type/radar backscatter class, these are approximations only.

[37] With this caveat in mind, fast-ice volume is given by

$$A = (F_R \times 5.0\ \text{m}) + (F_s \times 1.0\ \text{m}),$$

where F_R = rough fast-ice area and F_S = smooth fast-ice area. Overall sea ice volume is given by

$$B = (S_I - F_R - F_S) \times 0.65\ \text{m},$$

where S_I = sea ice area. The 0.65-m thickness for overall East Antarctic sea ice is an approximation based on ship-based estimates acquired during eight voyages through East Antarctic sea ice in November [*Worby et al.*, 1998]. This value was derived by multiplying the mean thickness for undeformed sea ice of 0.36 m (n = 1129) by a ridging factor of 1.8, to account for the contribution of pressure ridging, as suggested by *Worby et al.* [1998]. The fast ice to overall sea ice volume ratio is then

$$A/(A + B).$$

[38] Results are given in Table 3. The average volume of fast ice (as a percentage of overall sea ice volume in November) across regions 1–9 in 1997 is 26.7%, while that across regions 3–11 in 1999 is 27.7%. The respective

Table 5. Summary of Fast-Ice Parameters Derived From the 1997 and 1999 Maps Shown in Figures 4, 5, and 10[a]

Parameter	1997	1999
Longitude range, °E	87.5–170.3	75.2–150.6
Length of mapped coastline, km	3840	3500
Smooth (1–120) fast ice,[b] km^2	109,938	111,598
Smooth % of total fast ice	67.5	66.4
Rough (120–230) fast ice,[b] km^2	52,850	56,470
Rough % of total fast ice	32.5	33.6
Total area, km^2	162,788	168,068
Equivalent offshore width, km	43	48

[a]Values in parentheses are image threshold ranges in bytes.
[b]See definition of backscatter signal threshold levels in main text.

values for overlapping regions 3–9 for 1997 and 1999 are 31.4% and 30.7%. Values range quite widely on a sector-by-sector basis from ~10% (in regions 1 and 2) to ~52% (in region 8). Moreover, little change is noted in certain regions between 1997 and 1999, i.e., regions 5, 7 and 9, while substantial change occurs in other regions, i.e., 3, 4 and 8. The change is not always of the same sign, i.e., sector 3 versus sector 4.

[39] This volume estimation is a first approximation only, and detailed analyses of satellite laser altimeter data are required to give more accurate measurements (assuming that accurate snow depth information is available). We also note that compared to most of Antarctica, the East Antarctic sector covered by our study typically has the minimum offshore extent of sea ice at maximum extent [*Gloersen et al.*, 1992]. As a result, the value of ~28% for the fractional volume of fast ice would likely be an upper limit compared to most other sectors around Antarctica.

4. Summary

[40] In this study, we have constructed the first high-resolution maps of fast-ice extent and types for the East Antarctic coast between ~75°E and 170°E for November of 1997 and 1999, using image cross-correlation techniques applied to RADARSAT ScanSAR data. Although these maps are essentially ''snapshots'' in time and natural synoptic-scale variability occurs, they form benchmarks for the study of future changes in fast-ice areal coverage and characteristics along an extensive part of the Antarctic coastline using similar satellite SAR data from current and future missions.

[41] The results also underline both the highly recurrent nature of fast ice and the high degree of spatiotemporal variability in its distribution. It is apparent from Figures 10 and 11 that the distribution of East Antarctic fast ice exhibits high spatial variability, with offshore extent varying from a few kilometers in certain regions to ~200 km, for example, to the east of the Mertz Glacier. Bathymetry plays a key role via its impact on iceberg grounding, with icebergs acting as ''anchor points'' for fast-ice formation. In this respect, assemblages of small icebergs are as important, if not more important, than large icebergs.

[42] Two classes of fast ice have also been identified and mapped in the calibrated SAR imagery, based upon the radiometric stability of fast ice. In general, consistency is noted in the backscatter characteristics and distribution of the fast-ice types from 1997 and 1999. While little overall change is observed in (1) total fast-ice extent and (2) the relative proportions of the two major fast-ice types present in 1999 compared to 1997, there is considerable zonal variability. This is related largely to changes in the extent of ''smooth,'' i.e., annual, ice. Certain regions undergo considerable interannual variability in ''rough ice'' distribution. For example the ''wedge'' of fast-ice associated with grounded iceberg B-9B at ~147.5°E and the associated myriad of small bergs grounded on Ninnis Bank to the NE is extensive in November 1999 but less so in 1997. Comparing the maps from 1997 and 1999, the largest changes occur in the sectors from ~117°E to 151°E, with areas to the west exhibiting relatively little change.

[43] Using the new information on fast-ice areal extent and type combined with in situ observations of ice thickness as a function of type, we estimate that although fast ice forms only ~2–16% of total sea ice in November by area in the East Antarctic sector 75.15°E–170.30°E (average of ~8.3% across maps), it constitutes about 28% of the ice by volume (average across maps), but with a large range of ~10–52% across the individual regions. While this is an approximation only, based upon a number of basic assumptions about sea ice thickness as a function of radar backscatter-based ice classification, it underlines the key role of fast ice as a major store (reservoir) of ocean freshwater, with changes in fast-ice distribution in response to climate change/variability having major implications for the ocean freshwater budget. Encouragingly, fast-ice volume percen-

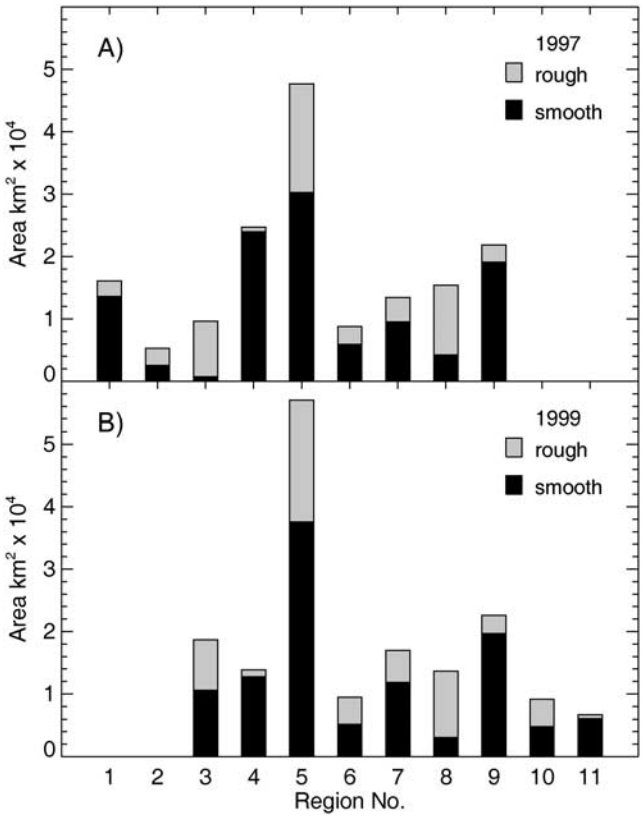

Figure 11. Areas of ''smooth'' and ''rough'' fast-ice types in the Novembers of (a) 1997 and (b) 1999, for the regions in Figures 4, 5, and 10. The fast-ice data are given in Table 4.

tages are very similar in both years studied, i.e., 26.7% versus 27.7%.

[44] The results presented here are "snapshot" estimates only, and more work is required to determine longer-term spatiotemporal variability. Moreover, the study could be spatially expanded to encompass the entire Antarctic coastal zone, subject to image availability. It is anticipated that the new multipolarization (Envisat ASAR) and fully polarimetric SAR data, for example, ALOS PALSAR and RADARSAT-2 SAR, will improve the discrimination of fast-ice types [*Lubin and Massom*, 2006], to enable more accurate proxy estimates of fast-ice volume. This in turn requires the collection of detailed in situ measurements for validation to relate fast-ice thickness to microwave signature. Improved "direct" measurements of thickness will result from analysis of satellite laser data from NASA's ICESat mission [*Yi and Zwally*, 2007]. Cloud-free data from the EOS Terra Multiangle Imaging Spectro-Radiometer (MISR) may also prove to be useful by enabling discrimination of fast-ice types based upon their surface roughness characteristics [*Nolin et al.*, 2002]. A key factor is the need for much improved bathymetric information in the coastal zone of Antarctic, a major challenge given that the region is covered by sea ice for much of the year, and in certain regions, perennially.

[45] **Acknowledgments.** This work was carried out with the support of the Australian Government's Cooperative Research Centres Programme through the Antarctic Climate and Ecosystems Cooperative Research Centre (ACE CRC). RADARSAT SAR data (courtesy of the Canadian Space Agency and RADARSAT International) were obtained from NASA grant NRA-99-OES-10, and processed by the Alaska Satellite Facility (Fairbanks, Alaska). SSM/I ice-concentration data were obtained from the NASA Earth Observing System Distributed Active Archive Center (DAAC) at the U. S. National Snow and Ice Data Center, University of Colorado, Boulder (http://nsidc.org). We thank Tony Sprent for advice concerning the representation of East Antarctica as a linear style map, Rick Porter-Smith (CSIRO Marine and Atmospheric Research, Australia) for providing bathymetric data, and Bill Budd and Jan Lieser (ACE CRC) for their excellent suggestions.

References

Arrigo, K. R., and G. L. van Dijken (2003), Phytoplankton dynamics within 37 Antarctic coastal polynya systems, *J. Geophys. Res.*, *108*(C8), 3271, doi:10.1029/2002JC001739.

Arrigo, K. R., J. N. Kremer, and C. W. Sullivan (1993), A simulated Antarctic fast-ice ecosystem, *J. Geophys. Res.*, *98*(C4), 6929–6946.

Bindoff, N. L., S. R. Rintoul, and R. Massom (2000), Polynyas and Bottom Water formation south of Tasmania, *Pap. Proc. R. Soc. Tasmania*, *133*(3), 51–56.

Bindschadler, R. A., and T. A. Scambos (1991), Satellite-image-derived velocity field of an Antarctic ice stream, *Science*, *252*, 242–246.

Comiso, J. C. (1995), SSM/I concentrations using the Bootstrap algorithm, *NASA Ref. Publ., 1380*, 40 pp.

Crocker, G. B., and P. Wadhams (1989), Breakup of Antarctic fast ice, *Cold Reg. Sci. Technol.*, *17*(1), 61–76.

Enomoto, H., F. Nishio, H. Warashina, and S. Ushio (2002), Satellite observation of melting and break-up of fast ice in Lützow-Holm Bay, East Antarctica, *Polar Meteorol. Glaciol.*, *16*, 1–14.

Fedotov, V. I., N. V. Cherepanov, and K. P. Tyshko (1998), Some features of the growth, structure and metamorphism of East Antarctic landfast sea ice, in *Antarctic Sea Ice Physical Processes, Interactions and Variability, Antarct. Res. Ser.*, vol. 74, edited by M. O. Jeffries, pp. 343–354, AGU, Washington. D. C.

Frezzotti, M., A. Cimbelli, and J. G. Ferrigno (1998), Ice-front and iceberg behaviour along Oates and George V coasts, Antarctica, 1912–96, *Ann. Glaciol.*, *27*, 643–650.

Garrison, D. L. (1991), Antarctic sea ice biota, *Am. Zool.*, *31*, 17–33.

Gloersen, P., W. J. Campbell, D. J. Cavalieri, J. G. Comiso, C. L. Parkinson, and H. J. Zwally (1992), Arctic and Antarctic sea ice, 1978–1987: Satellite passive-microwave observations and analysis, *NASA Spec. Publ., SP-511*, 290 pp.

Gray, A. L., K. E. Matar, P. W. Vachon, R. Bindschadler, K. C. Jezek, and R. Forster (1998), InSAR results from the RADARSAT Antarctic Mapping Mission data: Estimation of glacier motion using a simple registration procedure, paper presented at International Geoscience and Remote Sensing Symposium IGARSS'98, Inst. of Electr. and Electron. Eng., New York.

Heil, P. (2006), Atmospheric conditions and fast ice at Davis Station, East Antarctica: A case study, *J. Geophys. Res.*, *111*, C05009, doi:10.1029/2005JC002904.

Heil, P., I. Allison, and V. I. Lytle (1996), Seasonal and interannual variations of the oceanic heat flux under a landfast Antarctic sea ice cover, *J. Geophys. Res.*, *101*(C11), 25,741–25,752.

Keys, H. J. R. (1994), Ice giants a chip off the old B9, *Austr. Geogr. Mag.*, *33*, 22–23.

Kirkwood, R., and G. Robertson (1997), Seasonal change in the foraging ecology of Emperor penguins on the Mawson Coast, Antarctica, *Mar. Ecol. Prog. Ser.*, *156*, 205–223.

Kooyman, G. L., and J. Burns (1999), Weddell seal versus Emperor penguin: Boss of the Ross Sea, *Am. Zool.*, *39*, 9–19.

Kozlovsky, A. M., Y. L. Nazintsev, V. I. Fedotov, and N. V. Cherepanov (1977), Fast ice of the Eastern Antarctic (in Russian), *Proc. Sov. Antarct. Exped.*, *63*, 1–129.

Langhorne, P., V. A. Squire, C. Fox, and T. G. Haskell (2001), Lifetime estimation for a land-fast ice sheet subjected to ocean swell, *Ann. Glaciol.*, *33*, 333–338.

Lubin, D., and R. A. Massom (2006), *Polar Remote Sensing*, vol. 1, *Atmosphere and Polar Oceans*, 756 pp., Praxis/Springer, Chichester, U.K.

Martyn, P., J. Williams, J. Nicoll, R. Guritz, and T. Bicknell (1999), Calibration of the RADARSAT SWB Processor at the Alaska SAR Facility, paper presented at International Geoscience and Remote Sensing Symposium IGARSS'99, Inst. of Electr. and Electron. Eng., New York.

Massom, R. A. (2003), Recent iceberg calving events in the Ninnis Glacier region, *East Antarctica, Antarct. Sci.*, *15*(2), 303–313.

Massom, R. A., P. T. Harris, K. Michael, and M. J. Potter (1998a), The distribution and formative processes of latent heat polynyas in East Antarctica, *Ann. Glaciol.*, *27*, 420–426.

Massom, R. A., V. I. Lytle, A. P. Worby, and I. Allison (1998b), Winter snow cover variability on East Antarctic sea ice, *J. Geophys. Res.*, *103*(C11), 24,837–24,855.

Massom, R. A., K. L. Hill, V. I. Lytle, A. P. Worby, M. J. Paget, and I. Allison (2001a), Effects of regional fast-ice and iceberg distributions on the behaviour of the Mertz Glacier polynya, *East Antarctica, Ann. Glaciol.*, *33*, 391–398.

Massom, R. A., et al. (2001b), Snow on Antarctic sea ice, *Rev. Geophys.*, *39*(3), 413–445.

Massom, R. A., K. Jacka, M. J. Pook, C. Fowler, N. Adams, and N. Bindoff (2003), An anomalous late-season change in the regional sea ice regime in the vicinity of the Mertz Glacier Polynya, East Antarctica, *J. Geophys. Res.*, *108*(C7), 3212, doi:10.1029/2002JC001354.

McMinn, A., C. Ashworth, and K. G. Ryan (2000), In situ primary production of an Antarctic fast ice bottom algal community, *Aquat. Microb. Ecol.*, *21*, 177–185.

Morris, K., S. Li, and M. Jeffries (1999), Meso- and micro-scale sea-ice motion in the East Siberian Sea as determined from ERS-1 SAR data, *J. Glaciol.*, *45*(150), 370–383.

Murphy, E. J., A. Clarke, C. Symon, and J. J. Priddle (1995), Temporal variation in Antarctic sea-ice: Analysis of a long term fast-ice record from the South Orkney Islands, *Deep Sea Res., Part I*, *42*(7), 1045–1062.

Nolin, A. W., F. M. Fetterer, and T. A. Scambos (2002), Surface roughness characterizations of sea ice and ice sheets: Case studies with MISR data, paper presented at International Geoscience and Remote Sensing Symposium IGARSS'02, Inst. of Electr. and Electron. Eng., New York.

Olmsted, C. (1993), Alaska SAR facility scientific SAR user's guide, *ASF-SD-003*, 53 p., Alaska Satell. Fac., Fairbanks.

Porter-Smith, R. (2003), Bathymetry of the George Vth Land shelf and slope, *Deep Sea Res., Part II*, *50*(8)–(9), 1337–1341.

Rintoul, S. R. (1998), On the origin and influence of Adélie Land Bottom Water, in *Ocean, Ice and the Atmosphere: Interactions at the Antarctic Continental Margin, Antarct. Res. Ser.*, vol. 75, edited by S. Jacobs and R. Weiss, pp. 151–171, AGU, Washington, D. C.

Roberts, A., I. Allison, and V. I. Lytle (2001), Sensible and latent heat flux estimates over the Mertz Glacier Polynya from inflight measurements, *Ann. Glaciol.*, *33*, 377–384.

Ushio, S. (2006), Factors affecting fast-ice breakup frequency in Lützow-Holmbukta, Antarctica, *Ann. Glaciol.*, *44*, 177–182.

Worby, A. P., R. A. Massom, I. Allison, V. I. Lytle, and P. Heil (1998), East Antarctic sea ice: A review of its structure, properties and drift, in *Ant-*

arctic Sea Ice Physical Processes, Interactions and Variability, Antarct. Res. Ser., vol. 74, pp. 41–68, edited by M. O. Jeffries, AGU, Washington, D. C.

World Meteorological Organization (1970), The WMO sea-ice nomenclature: Terminology, codes and illustrated glossary, *WMO/OMM/BMO 259*, 145 pp., Geneva.

Yamanouchi, T., and K. Seko (1992), *Antarctica From NOAA Satellites: Clouds, Ice and Snow*, 91 pp., Natl. Inst. of Polar Res., Tokyo.

Yi, D., and H. J. Zwally (2007), Seasonal variation of Antarctic sea-ice freeboard height and thickness from ICESat, *Eos Trans. American Geophysical Union*, *85*(47), Abstract C33B-0346.

A. B. Giles and R. A. Massom, Antarctic Climate and Ecosystems Cooperative Research Centre, Private Bag 80, c/o University of Tasmania, Hobart, Tasmania 7001, Australia. (barry.giles@utas.edu.au; r.massom@utas.edu.au)

V. I. Lytle, Norwegian Polar Institute, Polar Environmental Centre, N-9296 Tromso, Norway. (vicky@npolar.no)